Two-port quantum model of finite-length transmission lines coupled to lumped circuits

Carlo Forestiere
Department of Electrical Engineering and Information Technology, Università degli Studi di Napoli Federico II, via Claudio 21, Naples, 80125, Italy

Giovanni Miano
Department of Electrical Engineering and Information Technology, Università degli Studi di Napoli Federico II, via Claudio 21, Naples, 80125, Italy

(Received 7 January 2024; accepted 14 March 2024; published 8 April 2024)

We show that, in the framework of quantum circuit electrodynamics in the Heisenberg picture, a finite-length transmission line can be described as a two-port lumped element of Thévenin type. Each port consists of a resistor connected in series to a controlled voltage source. The resistance of the resistors is equal to the characteristic impedance of the line. The controlled voltage sources are governed by linear equations with delay that take into account the reflections at the line ends. We apply this model to a transmission line capacitively coupled to two lumped circuits and obtain the reduced system of Heisenberg equations that governs them. Then, we show these equations can be reformulated as a pair of quantum Langevin-like equations that are coupled through the controlled voltage sources. Finally, we apply our approach to an analytically solvable network. This approach may be useful for the modeling of quantum links between superconducting circuits.

DOI: 10.1103/PhysRevA.109.043706

I. INTRODUCTION

The transmission line paradigm (e.g., Ref. [1]) holds a pivotal role in the domain of circuit quantum electrodynamics (e.g., Refs. [2–5]). This paradigm finds application in the modeling of one-dimensional resonators, wiring systems designed for control and measurement, and modeling of losses stemming from interactions with the surrounding environment. A substantial body of literature exists on methods for the quantization of superconducting networks, encompassing distributed circuits, transmission lines, and general impedance environments coupled with lumped circuits. A comprehensive summary of these methods is provided in Ref. [6].

Recent experimental studies have focused on systems comprising transmon qubits connected by transmission lines [7–13]. A primary objective of these studies is to develop a network of quantum processors, a crucial step for distributed quantum computers. This strategy shows promise in scaling quantum computing [9]. Such systems have also been instrumental in examining phenomena such as the violation of Bell's inequality [14,15].

Finite-length transmission lines, which are pivotal in these setups, may operate in various regimes. They can act as a short-range link connecting lumped elements [16,17], can be used in the implementation of LC resonators [16,17], and may serve as long-range links [9].

A finite-length transmission line can be modeled by using different approaches. In the discrete approach, the transmission line is represented as a cascade of discrete lumped elements, i.e., inductors and capacitors (e.g., Refs. [18–21]). In the mode expansion approach, the field operators associated to the transmission line are expanded into a well-suited set of modes (e.g., Refs. [3,6,22]). In the multiport impedance matrix approach, the finite-length transmission line is described as a two-port, then an equivalent lumped element two-port is synthesized by using classical circuit theory techniques (e.g., Refs. [16,23,24]). The multiport impedance matrix approach is general purpose and can be applied to any system composed of N nonlinear lumped elements interacting via a general time-dispersive linear distributed subsystem.

In this paper, we consider a finite-length transmission line coupled to two lumped circuits. We propose a two-port model of the transmission line in the Heisenberg picture, which extends the one-port model, which is commonly used in the literature for semi-infinite transmission lines (e.g., Refs. [4,25,26]). The two-port is composed of two resistors and two controlled sources. The resistance of the resistors is equal to the characteristic impedance of the line. The controlled sources are governed by linear equations with delay that take into account the reflections at the line ends. Using this model, we derive the reduced system of Heisenberg equations that govern the entire network. Eventually, we recast the reduced system into a quantum Langevin-like form. In the Markovian limit, this formulation is consistent with the model developed by Cirac *et al.* [27] to describe quantum transmission between atoms located at spatially separated nodes of a quantum network, which was later heuristically applied to describe transmon qubits connected by a transmission line [14]. The Cirac *et al.* model builds upon the input formalism developed by Gardiner [25,28].

The paper is organized as follows. In Sec. II, we first summarize a possible quantization approach for a semi-infinite transmission line linked to a lumped circuit via a single capacitor. Subsequently, in Sec. III we extend the approach

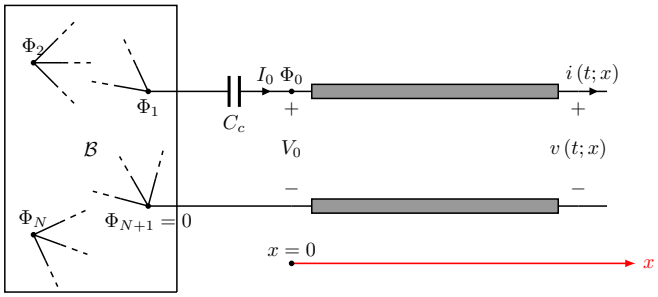

FIG. 1. A semi-infinite transmission line coupled to a lumped circuit $\mathcal{B}$ through the linear capacitor C_c.

to a finite-length transmission line capacitively coupled to two lumped circuits and derive the Heisenberg equations of motion. In Sec. IV, we derive an equivalent two-port model of the line that generalizes the equivalent one-port model for semi-infinite transmission lines. We introduce an equivalent lumped network with delay, give the reduced system of Heisenberg equations that governs the equivalent lumped circuit of the entire network, and reformulate them in a quantum Langevin-like form. In Sec. V, we apply the proposed equivalent model to study an analytically solvable network. Finally, we summarize our findings and discuss their implications in Sec. VI.

II. SEMI-INFINITE TRANSMISSION LINE

To streamline the presentation of the Heisenberg equations for a finite-length transmission line capacitively coupled to two lumped circuits, we summarize the key findings concerning a semi-infinite transmission line linked to a lumped circuit, as shown in Fig. 1 [29]. We provide the Lagrangian and Euler-Lagrange equations. Subsequently, we give the conjugate momenta and the Hamiltonian, and finally, we present the Heisenberg equations of motion. The results align with those that we would obtain by considering a discretized semi-infinite line and then taking the continuum limit, as done in Ref. [19].

Figure 1 shows a semi-infinite transmission line coupled to the lumped circuit $\mathcal{B}$ via C_c. The lumped circuit $\mathcal{B}$ contains linear capacitors and inductors, either linear or nonlinear. At every node of $\mathcal{B}$ at least one capacitor and one inductor meet. The entire network has $(N+2)$ nodes, numbered 0 to $N+1$. The coupling capacitor C_c is connected to the nodes 0 and 1, and the transmission line is connected to the nodes 0 and $N+1$. We indicate the node fluxes as $\Phi_0(t)$, $\Phi_1(t)$, …, $\Phi_N(t)$, $\Phi_{N+1}(t)$ where $\Phi_{N+1}=0$. The voltage of the branch h connected to the nodes i and j is $(\dot\Phi_i-\dot\Phi_j)$, where the dot denotes the ordinary time derivative.

The fundamental electrical variables of the semi-infinite transmission line are the current intensity $i(t;x)$ and the voltage $v(t;x)$, where $0\leqslant x<\infty$. The line inductance per unit length is ℓ, and capacitance per unit length is c. We introduce the field $\phi(t;x)=\int_{-\infty}^{t}v(\tau;x)d\tau$, so $v=\phi_t$ and $i=-\phi_x/\ell$ where $\phi_t\equiv\partial\phi/\partial t$ and $\phi_x\equiv\partial\phi/\partial x$. We describe the coupling between the transmission line and the lumped circuit through the boundary conditions

$$v(t;x=0)=V_0(t), \tag{1a}$$

$$i(t;x=0)=I_0(t), \tag{1b}$$

where $I_0(t)$ is the current intensity through the coupling capacitor C_c and $V_0(t)$ is the voltage at the end $x=0$ of the line, according to the reference current direction shown in Fig. 1. Since $V_0=\dot\Phi_0$, the boundary condition 1a is satisfied by imposing $\phi(t;x=0)=\Phi_0(t)$. As we will see, the other boundary condition arises directly from the Euler-Lagrange equations of the system.

A. Lagrangian and Euler-Lagrange equations

The Lagrangian L of the entire network consists of three distinct contributions: the contribution L_b of the lumped circuit $\mathcal{B}$, the contribution $L_{\rm tml}$ of the transmission line, and the contribution $L_{\rm cpl}$ describing the coupling between $\mathcal{B}$ and the transmission line through the capacitor C_c,

$$L=L_b+L_{\rm tml}+L_{\rm cpl}. \tag{2}$$

We introduce the N-dimensional column vector $\mathbf{\Phi}=|\Phi_1,\Phi_2,\ldots,\Phi_N|^{\intercal}$, which describes the degrees of freedom of $\mathcal{B}$. We denote by C_{rs} the capacitance of the capacitor that connects nodes r and s with $r,s=1,2,\ldots,N+1$, with $C_{rs}=0$ in cases where there is no capacitor between these nodes. We introduce the $(N+1)\times(N+1)$ capacitance matrix $[\mathbf{C}]$, whose nondiagonal elements are $-C_{rs}$ and the diagonal elements are equal to the opposite of the sum of values in the corresponding row or column. Subsequently, we introduce the matrix $[\mathbf{C}_b]$, which is derived from $[\mathbf{C}]$ by excluding both the row and column corresponding to the $(N+1)$th node (the ground node). The contribution L_b to the Lagrangian is given by

$$L_b=\tfrac{1}{2}\dot{\mathbf{\Phi}}^{\intercal}[\mathbf{C}_b]\dot{\mathbf{\Phi}}-U_b(\mathbf{\Phi}), \tag{3}$$

where $U_b=U_b(\mathbf{\Phi})$ is the potential energy of the circuit comprising the sum of energies stored in the inductors, whether linear or nonlinear. The degrees of freedom of the line are $\Phi_0(t)$ and $\phi(t;x)$ for $0<x<\infty$. The contribution $L_{\rm tml}$ is given by (e.g., Ref. [30])

$$L_{\rm tml}=\int_0^\infty dx\,\mathcal{L}_{\rm tml}(\phi_t,\phi_x), \tag{4}$$

where

$$\mathcal{L}_{\rm tml}=\frac{c}{2}\phi_t^2-\frac{1}{2\ell}\phi_x^2 \tag{5}$$

is the Lagrangian density. The contribution $L_{\rm cpl}$ is given by

$$L_{\rm cpl}=\frac{C_c}{2}(\dot\Phi_1-\dot\Phi_0)^2. \tag{6}$$

The system of Euler-Lagrange equations for $\mathbf{\Phi}$ is

$$\frac{d}{dt}\frac{\partial}{\partial\dot{\mathbf{\Phi}}}(L_b+L_{\rm cpl})-\frac{\partial L_b}{\partial\mathbf{\Phi}}=0. \tag{7}$$

The Euler-Lagrange equation for ϕ with $0<x<\infty$ is

$$\frac{\partial}{\partial t}\frac{\partial\mathcal{L}_{\rm tml}}{\partial\phi_t}+\frac{\partial}{\partial x}\frac{\partial\mathcal{L}_{\rm tml}}{\partial\phi_x}=0. \tag{8}$$

The Euler-Lagrange equations for Φ_0 is

$$\frac{d}{dt}\frac{\partial L_{\rm cpl}}{\partial \dot{\Phi}_0} + \frac{\partial \mathcal{L}_{\rm tml}}{\partial \phi_x}\bigg|_{x=0} = 0. \tag{9}$$

The degree of freedom Φ_0 is shared by the coupling capacitor and the transmission line and contributes to the first variation of the action through both $L_{\rm cpl}$ and $L_{\rm tml}$, [19,29]. In fact, $\frac{\partial \mathcal{L}_{\rm tml}}{\partial \phi_x}|_{x=0}\delta\Phi_0$ gives the contribution of the variation of Φ_0 to the variation of the Lagrangian.

Using the expressions of L_b and $L_{\rm cpl}$, from the Euler-Lagrange equation (7) we obtain

$$[\mathbf{C}_b]\frac{d^2\mathbf{\Phi}}{dt^2} + \frac{\partial U_b}{\partial \mathbf{\Phi}} + C_c\frac{d^2}{dt^2}(\Phi_1 - \Phi_0)\mathbf{1}_N = \mathbf{0}, \tag{10}$$

where $\mathbf{1}_N$ is the N-dimensional column vector $|1, 0, \ldots, 0, 0|^\intercal$. Using the expressions of $\mathcal{L}_{\rm tml}$, from the Euler-Lagrange equation (8) we obtain the wave equation for the flux field for $0 < x < \infty$,

$$\frac{\partial^2\phi}{\partial t^2} - v_p^2\frac{\partial^2\phi}{\partial x^2} = 0, \tag{11}$$

where $v_p = 1/\sqrt{\ell c}$. Using the expressions of $L_{\rm cpl}$ and $\mathcal{L}_{\rm tml}$, from the Euler-Lagrange equation (9) we obtain

$$C_c\frac{d^2}{dt^2}(\Phi_1 - \Phi_0) + \frac{1}{\ell}\phi_x(t; x = 0) = 0. \tag{12}$$

The system of Eqs. (10) returns the Kirchhoff current law at the nodes $1, 2, \ldots, N$ of the lumped circuit $\mathcal{B}$. Since $i(t; x = 0) = -\phi_x(t; x = 0)/\ell$, combining Eqs. (12) and the characteristic equation of the capacitor C_c, we obtain the boundary condition (1b).

B. Conjugate variables and Hamiltonian

The conjugate momentum to $\mathbf{\Phi}$ is

$$\mathbf{Q} = \frac{\partial}{\partial \dot{\mathbf{\Phi}}}(L_b + L_{\rm cpl}) = [\mathbf{C}_b]\dot{\mathbf{\Phi}} + C_c(\dot{\Phi}_1 - \dot{\Phi}_0)\mathbf{1}_N, \tag{13}$$

according to Eq. (7). The conjugate momentum to ϕ is for $0 < x < \infty$

$$q = \frac{\partial \mathcal{L}_{\rm tml}}{\partial \phi_t} = c\,\phi_t, \tag{14}$$

according to Eq. (8). The conjugate momentum to Φ_0 is

$$Q_0 = \frac{\partial L_{\rm cpl}}{\partial \dot{\Phi}_0} = -C_c(\dot{\Phi}_1 - \dot{\Phi}_0), \tag{15}$$

according to Eq. (9). Combining Eqs. (13) and (15) we obtain

$$\dot{\mathbf{\Phi}} = [\mathbf{C}_b]^{-1}(\mathbf{Q} + Q_0\mathbf{1}_N), \tag{16}$$

and

$$\dot{\Phi}_0 = \mathbf{p}^\intercal\mathbf{Q} + \frac{1}{C_p}Q_0, \tag{17}$$

where $\mathbf{p}$ is the N-dimensional column vector with elements $p_j = ([\mathbf{C}_b]^{-1})_{1,\,j}$ for $j = 1, 2, \ldots, N$ (i.e., the elements of the first row of $[\mathbf{C}_b]^{-1}$) and

$$\frac{1}{C_p} = \frac{1}{C_c} + p_1. \tag{18}$$

Since the matrix $[\mathbf{C}_b]$ is symmetric, we have $[\mathbf{C}_b]\mathbf{p} = \mathbf{1}_N$.

The Hamiltonian of the entire network is the sum of the energies stored within the circuit $\mathcal{B}$, the coupling capacitor, and the transmission line. In terms of the degrees of freedom and their conjugate momenta introduced above, it is given by:

$$H = H_b + H_{\rm tml} + H_{\rm cpl}, \tag{19}$$

where

$$H_b = \frac{1}{2}\mathbf{Q}^\intercal[\mathbf{C}_b]^{-1}\mathbf{Q} + U_c(\mathbf{\Phi}), \tag{20a}$$

$$H_{\rm cpl} = \mathbf{p}^\intercal\mathbf{Q}Q_0 + \frac{1}{2C_p}Q_0^2, \tag{20b}$$

$$H_{\rm tml} = \int_0^\infty \left(\frac{1}{2c}q^2 + \frac{1}{2\ell}\phi_x^2\right)dx. \tag{20c}$$

C. Heisenberg equations of motion

We now promote the conjugate variables $(\mathbf{\Phi}, \mathbf{Q})$, (Φ_0, Q_0), (ϕ, q), and H to operators. In the Heisenberg picture, the equal-time commutation relations are

$$[\hat{\Phi}_k(t), \hat{Q}_k(t)] = i\hbar \quad \text{for } k = 1, 2, \ldots, N, \tag{21a}$$

$$[\hat{\Phi}_0(t), \hat{Q}_0(t)] = i\hbar, \tag{21b}$$

$$[\hat{\phi}(t; x'), \hat{q}(t; x)] = i\hbar\delta(x' - x) \quad \text{for } 0 < x < \infty, \tag{21c}$$

while all remaining equal-time commutators vanish. The Heisenberg equations for the conjugate operators $(\hat{\mathbf{\Phi}}, \hat{\mathbf{Q}})$ are

$$\dot{\hat{\mathbf{\Phi}}} = \frac{1}{i\hbar}[\hat{\mathbf{\Phi}}, \hat{H}] = [\mathbf{C}_b]^{-1}(\hat{\mathbf{Q}} + \mathbf{1}_N\hat{Q}_0), \tag{22a}$$

$$\dot{\hat{\mathbf{Q}}} = \frac{1}{i\hbar}[\hat{\mathbf{Q}}, \hat{H}] = -\frac{\partial U_b}{\partial \hat{\mathbf{\Phi}}}. \tag{22b}$$

The Heisenberg equations for the conjugate operators $(\hat{\Phi}_0, \hat{Q}_0)$ are

$$\dot{\hat{\Phi}}_0 = \frac{1}{i\hbar}[\hat{\Phi}_0, \hat{H}] = \mathbf{p}^\intercal\hat{\mathbf{Q}} + \frac{1}{C_p}\hat{Q}_0, \tag{23a}$$

$$\dot{\hat{Q}}_0 = \frac{1}{i\hbar}[\hat{Q}_0, \hat{H}] = \frac{1}{\ell}\hat{\phi}_x(t; x = 0). \tag{23b}$$

Lastly, the Heisenberg equations for the conjugate operators $(\hat{\phi}, \hat{q})$, with $0 < x < \infty$, are

$$\hat{\phi}_t = \frac{1}{i\hbar}[\hat{\phi}, \hat{H}] = \frac{1}{c}\hat{q}, \tag{24a}$$

$$\hat{q}_t = \frac{1}{i\hbar}[\hat{q}, \hat{H}] = \frac{1}{\ell}\hat{\phi}_{xx}, \tag{24b}$$

where $\hat{\phi}_{xx} \equiv \partial^2\hat{\phi}/\partial x^2$. We recall $\hat{\phi}(t; x = 0) = \hat{\Phi}_0(t)$. The Heisenberg equations must be solved with the initial condition that, at the initial time, any operator in the Heisenberg picture should be equal to the corresponding operator in the Schrödinger picture, denoted as $\hat{O}^{(S)}$.

Combining Eqs. (22a), (22b), and (23a), applying the relation $[\mathbf{C}_b]\mathbf{p} = \mathbf{1}_N$, we obtain

$$[\mathbf{C}_b]\frac{d^2\hat{\mathbf{\Phi}}}{dt^2} + \frac{\partial U_b}{\partial \hat{\mathbf{\Phi}}} + C_c\frac{d^2}{dt^2}(\hat{\Phi}_1 - \hat{\Phi}_0)\mathbf{1}_N = \mathbf{0}. \tag{25}$$

From Eqs. (23a), (23b), and (22a) we also obtain

$$C_c\frac{d^2}{dt^2}(\hat{\Phi}_1 - \hat{\Phi}_0) + \frac{1}{\ell}\hat{\phi}_x(t; x = 0) = 0. \tag{26}$$

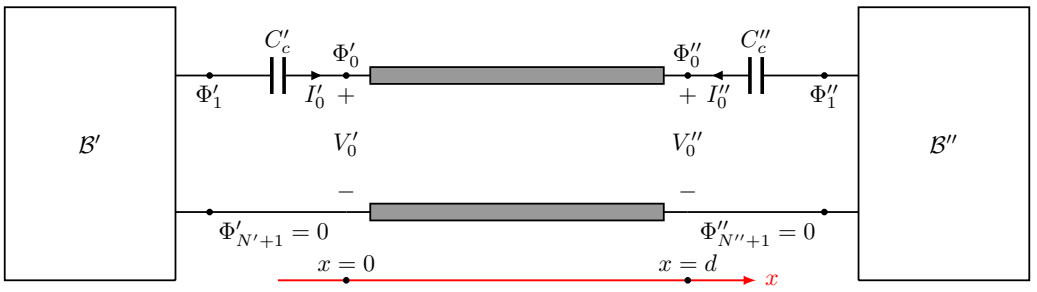

FIG. 2. A network composed of a finite length transmission line capacitively coupled to the lumped circuits $\mathcal{B}'$ and $\mathcal{B}''$ through the linear capacitors C_c' and C_c''. The reference directions for the voltage $v(t;x)$ and the current intensity $i(t;x)$ are the same as those indicated in Fig. 1 for the semi-infinite line.

Lastly, from Eqs. (24a) and (24b) we obtain for $0 < x < \infty$

$$\frac{\partial^2 \hat{\phi}}{\partial t^2} - v_p^2 \frac{\partial^2 \hat{\phi}}{\partial x^2} = 0. \tag{27}$$

The system of Eqs. (25)–(27) are the quantized version of the system of Eqs. (10)–(12).

III. FINITE LENGTH TRANSMISSION LINE

We now consider a transmission line of length d that is capacitively coupled to the lumped circuits $\mathcal{B}'$ and $\mathcal{B}''$ through the capacitors C_c' and C_c'', as shown in Fig. 2. Building on the results obtained for the semi-infinite line, we can readily derive the Lagrangian and Hamiltonian formulations, as well as the quantization and Heisenberg equations of motion for the observables of the entire system.

The lumped circuits $\mathcal{B}'$ and $\mathcal{B}''$ have the same characteristics as the lumped circuit $\mathcal{B}$ considered in the previous section. In particular, $\mathcal{B}'$ has $(N'+1)$ nodes and $\mathcal{B}''$ has $(N''+1)$ nodes. The capacitor C_c' is connected to the nodes $0'$ and $N'+1$, while the capacitor C_c'' is connected to the nodes $0''$ and $N''+1$. The transmission line is connected to the nodes $0'$ and $N'+1$ on the left, and to the nodes $0''$ and $N''+1$ on the right. As in the case of the semi-infinite line, we apply the node method (e.g., Ref. [4]). We indicate the flux associated with the node i' by $\Phi_i'(t)\ \forall i' \in [1, N'+1]$, and the flux associated to the node i'' by $\Phi_i''(t)\ \forall i'' \in [1, N''+1]$. We set $\Phi_{N'+1}' = 0$ and $\Phi_{N''+1}'' = 0$. We denote the set of node fluxes of $\mathcal{B}'$ by the N'-dimensional column vector $\mathbf{\Phi}'$ and the set of node fluxes of $\mathcal{B}''$ by the N''-dimensional column vector $\mathbf{\Phi}''$. The lumped circuit $\mathcal{B}'$ is characterized by the $(N' \times N')$ capacitance matrix $[\mathbf{C}_b']$ and the potential energies $U_b' = U_b'(\mathbf{\Phi}')$; the lumped circuit $\mathcal{B}''$ is characterized by the $(N'' \times N'')$ capacitance matrix $[\mathbf{C}_b'']$ and the potential energies $U_b'' = U_b''(\mathbf{\Phi}'')$.

The electrical variables of the transmission line are defined over the interval $0 \leqslant x \leqslant d$. We describe the coupling of the line with the two lumped circuits by the boundary conditions

$$v(t;x=0) = V_0'(t), \quad v(t;x=d) = V_0''(t), \tag{28a}$$

$$i(t;x=0) = I_0'(t), \quad i(t;x=d) = -I_0''(t), \tag{28b}$$

where $I_0'(t)$ is the current intensity through the coupling capacitor C_c', $I_0''(t)$ is the current intensity through the coupling capacitor C_c'', $V_0'(t)$ is the voltage at the left end of the line, $V_0''(t)$ is the voltage at the right end of the line, according to the reference versus shown in Fig. 2. Since $V_0' = \dot{\Phi}_0'$ and $V_0'' = \dot{\Phi}_0''$, the boundary conditions for the voltages are satisfied by imposing

$$\phi(t;x=0) = \Phi_0'(t), \quad \phi(t;x=d) = \Phi_0''(t). \tag{29}$$

As for the semi-infinite transmission line, the other boundary conditions are naturally imposed through the formulation of the problem.

A. Lagrangian

The degrees of freedom of the whole system are $\mathbf{\Phi}'(t)$, $\Phi_0'(t)$, $\phi(t;x)$ for $0 < x < d$, $\Phi_0''(t)$, and $\mathbf{\Phi}''(t)$. The Lagrangian is

$$L = L_b' + L_b'' + L_{\text{tml}} + L_{\text{cpl}}' + L_{\text{cpl}}'', \tag{30}$$

where L_b' and L_b'' give the contribution of $\mathcal{B}'$ and $\mathcal{B}''$, L_{tml} gives the contribution of the line, L_{cpl}' and L_{cpl}'' take into account the capacitive coupling between the line and the lumped circuits $\mathcal{B}'$ and $\mathcal{B}''$. The expressions of L_b' and L_b'' are of the same type as those given by Eq. (3), $L_b' = \frac{1}{2}\dot{\mathbf{\Phi}}'^{\intercal}[\mathbf{C}_b']\dot{\mathbf{\Phi}}' - U_b'(\mathbf{\Phi}')$ and $L_b'' = \frac{1}{2}\dot{\mathbf{\Phi}}''^{\intercal}[\mathbf{C}_b'']\dot{\mathbf{\Phi}}'' - U_b''(\mathbf{\Phi}'')$. The expressions of L_{cpl}' and L_{cpl}'' are of the same type as those given by Eq. (6), $L_{\text{cpl}}' = \frac{C_c'}{2}(\dot{\Phi}_1' - \dot{\Phi}_0')^2$ and $L_{\text{cpl}}'' = \frac{C_c''}{2}(\dot{\Phi}_1'' - \dot{\Phi}_0'')^2$. The expression of the contribution of the line is $L_{\text{tml}} = \int_0^d dx\, \mathcal{L}_{\text{tml}}(\phi_t, \phi_x)$ where the Lagrangian density $\mathcal{L}_{\text{tml}}$ is given by (5).

The Euler-Lagrange equations for $\mathbf{\Phi}'$ and $\mathbf{\Phi}''$ share the same form as those presented in (10); however, it is necessary to note that the reference directions for I_0'' and $i(t;x=d)$ are different. The Euler-Lagrange equation for $\phi(t;x)$ is given by (11) where $0 < x < d$. The Euler-Lagrange equations for Φ_0' and Φ_0'' are of the same type as those given by (12).

B. Conjugate variables and Hamiltonian

We denote by $\mathbf{Q}'(t)$ and $\mathbf{Q}''(t)$ the conjugate momenta to $\mathbf{\Phi}'(t)$ and $\mathbf{\Phi}''(t)$, and by $Q_0'(t)$ and $Q_0''(t)$ the conjugate momenta to $\Phi_0'(t)$ and $\Phi_0''(t)$. The expressions of $\mathbf{Q}'(t)$ and $\mathbf{Q}''(t)$ are of the same type as those given by (13), $\mathbf{Q}' = [\mathbf{C}_b']\dot{\mathbf{\Phi}}' + C_c'(\dot{\Phi}_1' - \dot{\Phi}_0')\mathbf{1}_{N'}$, and $\mathbf{Q}'' = [\mathbf{C}_b'']\dot{\mathbf{\Phi}}'' + C_c''(\dot{\Phi}_1'' - \dot{\Phi}_0'')\mathbf{1}_{N''}$; the vector $\mathbf{1}_{N'}$ is the N'-dimensional column vector $|1, 0, \ldots, 0, 0|^{\intercal}$, and the vector $\mathbf{1}_{N''}$ is defined in an analogously way. The expression $q(t;x)$ of the conjugate momenta to $\phi(t;x)$ is given by (14) where $0 < x < d$. Lastly, the expressions of $Q_0''(t)$ and $Q_0''(t)$ are of the same

type as those given by (15), $Q'_0 = -C'_c(\dot{\Phi}'_1 - \dot{\Phi}'_0)$ and $Q''_0 = -C''_c(\dot{\Phi}''_1 - \dot{\Phi}''_0)$.

The Hamiltonian of the entire network is

$$H = H'_b + H''_b + H_{\rm tml} + H'_{\rm cpl} + H''_{\rm cpl}, \tag{31}$$

where H'_b and H''_b account for the contribution of the lumped circuits $\mathcal{B}'$ and $\mathcal{B}''$, $H_{\rm tml}$ takes into account the contribution of the line, $H'_{\rm cpl}$ and $H''_{\rm cpl}$ take into account the interaction between the line and the lumped circuits $\mathcal{B}'$ and $\mathcal{B}''$. The expressions of H'_b and H''_b follow the same form as expressed in Eq. (20a), $H'_b = \frac{1}{2}\mathbf{Q}'^{\mathsf{T}}[\mathbf{C}'_b]^{-1}\mathbf{Q}' + U'_c(\mathbf{\Phi}')$ and $H''_b = \frac{1}{2}\mathbf{Q}''^{\mathsf{T}}[\mathbf{C}''_b]^{-1}\mathbf{Q}'' + U''_c(\mathbf{\Phi}'')$. The expression of $H_{\rm tml}$ is given by $H_{\rm tml} = \int_0^d dx(\frac{1}{2c}q^2 + \frac{1}{2\ell}\phi_x^2)$. Lastly, the expressions of $H'_{\rm cpl}$ and $H''_{\rm cpl}$ are of the same type as those given by (20b), $H'_{\rm cpl} = (\mathbf{p}'^{\mathsf{T}}\mathbf{Q}')Q'_0 + \frac{1}{2C'_p}Q'^2_0$ and $H''_{\rm cpl} = (\mathbf{p}''^{\mathsf{T}}\mathbf{Q}'')Q''_0 + \frac{1}{2C''_p}Q''^2_0$. The vector $\mathbf{p}'$ is the N'- dimensional column vector with elements $p'_j = ([\mathbf{C}_b]^{-1})_{1,j}$ for $j = 1, 2, \ldots, N'$, and the vector $\mathbf{p}''$ is defined analogously. The capacitances C'_p and C''_p are defined as $C'_p = C'_c/(1 + C'_c\, p'_1)$ and $C''_p = C''_c/(1 + C''_c\, p''_1)$ where p'_1 and p''_1 are the first elements of the vectors $\mathbf{p}'$ and $\mathbf{p}''$, respectively.

C. Heisenberg equations

We now promote the conjugate variables $(\mathbf{\Phi}', \mathbf{Q}')$, (Φ'_0, Q'_0), (ϕ, q) for $0 < x < d$, $(\mathbf{\Phi}'', \mathbf{Q}'')$, (Φ''_0, Q_0) and the Hamiltonian H to operators. In the Heisenberg picture, the equal-time commutation relations are of the same type as those given by (21a)–(21c), while all remaining equal-time commutators vanish. The Heisenberg equations for these operators are of the same type as those obtained for the semi-infinite transmission line in Sec. II C. The Heisenberg equations for the conjugate operators $(\hat{\mathbf{\Phi}}', \hat{\mathbf{Q}}')$ and the conjugate operators $(\hat{\mathbf{\Phi}}'', \hat{\mathbf{Q}}'')$ are

$$\dot{\hat{\mathbf{\Phi}}}' = [\mathbf{C}'_b]^{-1}\hat{\mathbf{Q}}' + \mathbf{p}'\hat{Q}'_0, \tag{32a}$$

$$\dot{\hat{\mathbf{Q}}}' = -\frac{\partial U'_b}{\partial \hat{\mathbf{\Phi}}'}, \tag{32b}$$

and

$$\dot{\hat{\mathbf{\Phi}}}'' = [\mathbf{C}''_b]^{-1}\hat{\mathbf{Q}}'' + \mathbf{p}''\hat{Q}''_0, \tag{33a}$$

$$\dot{\hat{\mathbf{Q}}}'' = -\frac{\partial U''_b}{\partial \hat{\mathbf{\Phi}}''}. \tag{33b}$$

The Heisenberg equations for the conjugate operators $(\hat{\Phi}'_0, \hat{Q}'_0)$ and the conjugate operators $(\hat{\Phi}''_0, \hat{Q}''_0)$ are

$$\dot{\hat{\Phi}}'_0 = \mathbf{p}'^{\mathsf{T}}\hat{\mathbf{Q}}' + \frac{1}{C'_p}\hat{Q}'_0, \tag{34a}$$

$$\dot{\hat{Q}}'_0 = \frac{1}{\ell}\hat{\phi}_x(t; x = 0), \tag{34b}$$

and

$$\dot{\hat{\Phi}}''_0 = \mathbf{p}''^{\mathsf{T}}\hat{\mathbf{Q}}'' + \frac{1}{C''_p}\hat{Q}''_0, \tag{35a}$$

$$\dot{\hat{Q}}''_0 = -\frac{1}{\ell}\hat{\phi}_x(t; x = d). \tag{35b}$$

Lastly, the Heisenberg equations for and the conjugate operators $(\hat{\phi}, \hat{q})$ are for $0 < x < d$:

$$\hat{\phi}_t = \frac{1}{c}\hat{q}, \tag{36a}$$

$$\hat{q}_t = \frac{1}{\ell}\hat{\phi}_{xx}, \tag{36b}$$

where $\hat{\phi}_{xx} \equiv \partial^2\hat{\phi}/\partial x^2$. In addition, we need to enforce the boundary conditions (29) for the operators, ensuring that $\hat{\phi}(t; x = 0)$ matches $\hat{\Phi}'_0(t)$, and $\hat{\phi}(t; x = d)$ matches $\hat{\Phi}''_0(t)$. The Heisenberg equations must be solved with the requirement that at $t = 0$ the operators in the Heisenberg picture are equal to their counterparts in the Schrödinger picture.

IV. TWO-PORT CHARACTERIZATION OF THE TRANSMISSION LINE

In the Heisenberg picture, a finite-length transmission line can be represented as a two-port element with electrical observables $(\hat{V}'_0, \hat{I}'_0)$ on the left port and $(\hat{V}''_0, \hat{I}''_0)$ on the right port. In this way, we can greatly simplify the system of Heisenberg equations (32a)–(36b), which govern the entire network.

To characterize the line as two-port, we begin by solving Eqs. (36a) and (36b) with the boundary conditions $\hat{\phi}(t; x = 0) = \hat{\Phi}'_0(t)$ and $\hat{\phi}(t; x = d) = \hat{\Phi}''_0(t)$. Subsequently, we express the current intensity operators at the ends of the line $\hat{I}'_0$ and $\hat{I}''_0$ as functions of the voltage operators $\hat{V}'_0$ and $\hat{V}''_0$, as well as the initial conditions.

A. Solution of the operator wave equation

By combining Eqs. (36a) and (36b), we obtain $\hat{\phi}_{tt} = v_p^2\,\hat{\phi}_{xx}$ for $0 < x < d$ where $\hat{\phi}_{tt} \equiv \partial^2\hat{\phi}/\partial t^2$. Its general solution can be expressed as

$$\hat{\phi}(t; x) = \hat{\phi}_{\rightarrow}\left(t - \frac{x}{v_p} + T\right) + \hat{\phi}_{\leftarrow}\left(t + \frac{x}{v_p}\right), \tag{37}$$

where the unknown field operators $\hat{\phi}_{\rightarrow} = \hat{\phi}_{\rightarrow}(t)$ and $\hat{\phi}_{\leftarrow} = \hat{\phi}_{\leftarrow}(t)$ are defined in the time interval $(0, +\infty)$, and $T = d/v_p$ is the one-way transit time. The operators $\hat{\phi}_{\rightarrow}$ and $\hat{\phi}_{\leftarrow}$ depend both on the initial conditions for the conjugate observables of the line and on the boundary conditions, which describe the interaction of the line with the lumped circuits.

From Eq. (36a) we obtain for the charge density field operator

$$\hat{q}(t; x) = c\left[\hat{v}_{\rightarrow}\left(t - \frac{x}{v_p} + T\right) + \hat{v}_{\leftarrow}\left(t + \frac{x}{v_p}\right)\right], \tag{38}$$

where we have introduced the operators $\hat{v}_{\rightarrow}(t)$ and $\hat{v}_{\leftarrow}(t)$ defined as $\hat{v}_{\rightarrow} \equiv \dot{\hat{\phi}}_{\rightarrow}$ and $\hat{v}_{\leftarrow} \equiv \dot{\hat{\phi}}_{\leftarrow}$. The voltage and current intensity field operators along the line are given by $\hat{q} = c\hat{v}$ and $\hat{i} = -\hat{\phi}_x/\ell$, thus from (37) and (38) we obtain

$$\hat{v}(t; x) = \hat{v}_{\rightarrow}\left(t - \frac{x}{v_p} + T\right) + \hat{v}_{\leftarrow}\left(t + \frac{x}{v_p}\right), \tag{39a}$$

$$\hat{i}(t; x) = \frac{1}{Z_c}\left[\hat{v}_{\rightarrow}\left(t - \frac{x}{v_p} + T\right) - \hat{v}_{\leftarrow}\left(t + \frac{x}{v_p}\right)\right], \tag{39b}$$

where $Z_c = \sqrt{\ell/c}$ is the characteristic impedance of the line. The operator $\hat{v}_{\rightarrow}(t)$ is the forward voltage wave

operator of the line at the end $x = d$; the operator $\hat{v}_{\leftarrow}(t)$ is the backward voltage wave operator of the line at the left end $x = 0$. The observables of the transmission line are entirely determined by $\hat{v}_{\rightarrow}$ and $\hat{v}_{\leftarrow}$, thus, they specify the state of the transmission line.

The initial conditions for the flux and charge density field operators are for $0 < x < d$

$$\hat{\phi}(t = 0; x) = \hat{\phi}^{(S)}(x), \tag{40a}$$

$$\hat{q}(t = 0; x) = \hat{q}^{(S)}(x), \tag{40b}$$

where $\hat{\phi}^{(S)}(x)$ and $\hat{q}^{(S)}(x)$ are the flux field operator and the charge density field operator in the Schrödinger picture. By imposing (40), we have for $0 < x < d$

$$\hat{\phi}_x^{(S)}(x) = \frac{1}{v_p}\left[-\dot{\hat{\phi}}_{\rightarrow}\left(T - \frac{x}{v_p}\right) + \dot{\hat{\phi}}_{\leftarrow}\left(\frac{x}{v_p}\right)\right], \tag{41a}$$

$$\hat{q}^{(S)}(x) = c\left[\dot{\hat{\phi}}_{\rightarrow}\left(T - \frac{x}{v_p}\right) + \dot{\hat{\phi}}_{\leftarrow}\left(\frac{x}{v_p}\right)\right]. \tag{41b}$$

These equations determine the forward and backward voltage operators in the time interval $(0, T)$. Indeed, we obtain for $0 < t < T$

$$\hat{v}_{\rightarrow}(t) = \hat{v}_{\rightarrow}^{(0)}(t), \tag{42a}$$

$$\hat{v}_{\leftarrow}(t) = \hat{v}_{\leftarrow}^{(0)}(t), \tag{42b}$$

where

$$\hat{v}_{\rightarrow}^{(0)}(t) = \frac{1}{2c}\left\{\hat{q}^{(S)}[v_p(T - t)] - \frac{1}{Z_c}\hat{\phi}_x^{(S)}[v_p(T - t)]\right\}, \tag{43a}$$

$$\hat{v}_{\leftarrow}^{(0)}(t) = \frac{1}{2c}\left[\hat{q}^{(S)}(v_p t) + \frac{1}{Z_c}\hat{\phi}_x^{(S)}(v_p t)\right]. \tag{43b}$$

B. Equivalent two-port

We now derive the characteristic relations of the two-port that describe the transmission line by applying the boundary conditions (28). Specifying expressions (39a) and (39b) at the line end $x = 0$ we obtain

$$\hat{V}_0'(t) = \hat{v}_{\rightarrow}(t + T) + \hat{v}_{\leftarrow}(t), \tag{44a}$$

$$Z_c\hat{I}_0'(t) = \hat{v}_{\rightarrow}(t + T) - \hat{v}_{\leftarrow}(t), \tag{44b}$$

whereas specifying them at the line end $x = d$, we obtain

$$\hat{V}_0''(t) = \hat{v}_{\rightarrow}(t) + \hat{v}_{\leftarrow}(t + T), \tag{45a}$$

$$-Z_c\hat{I}_0''(t) = \hat{v}_{\rightarrow}(t) - \hat{v}_{\leftarrow}(t + T). \tag{45b}$$

Subtracting Eqs. (44a) and (44b) termwise and by adding Eqs. (45a) and (45b) termwise, we have for $0 < t < \infty$

$$\hat{V}_0'(t) - Z_c\hat{I}_0'(t) = 2\hat{v}_{\leftarrow}(t), \tag{46a}$$

$$\hat{V}_0''(t) - Z_c\hat{I}_0''(t) = 2\hat{v}_{\rightarrow}(t). \tag{46b}$$

If $\hat{v}_{\rightarrow}(t)$ and $\hat{v}_{\leftarrow}(t)$ were known in any t, these equations would completely determine the terminal behavior of the line. From Eqs. (44a) and (45a) we obtain the equations that govern $\hat{v}_{\rightarrow}(t)$ and $\hat{v}_{\leftarrow}(t)$ for $0 < t < \infty$

$$\hat{v}_{\rightarrow}(t + T) = \hat{V}_0'(t) - \hat{v}_{\leftarrow}(t), \tag{47a}$$

$$\hat{v}_{\leftarrow}(t + T) = \hat{V}_0''(t) - \hat{v}_{\rightarrow}(t). \tag{47b}$$

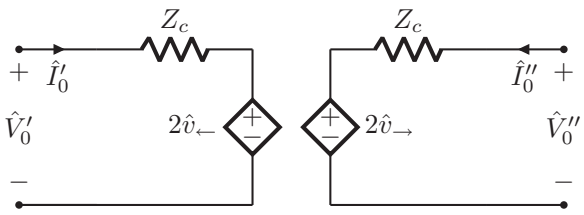

FIG. 3. Equivalent two-port of Thévenin type of finite-length transmission lines in the Heisenberg picture. The equations $\hat{v}_{\rightarrow}(t + T) = \hat{V}_0'(t) - \hat{v}_{\leftarrow}(t)$ and $\hat{v}_{\leftarrow}(t + T) = \hat{V}_0''(t) - \hat{v}_{\rightarrow}(t)$ control the two voltage sources for $0 < t < \infty$.

The set of equations (46a)–(47b) describes the terminal properties of the line, as well as its state. Equations (47a) and (47b) govern the evolution of the state variables of the line. They must be solved with the initial conditions (42) for $0 < t < T$.

Equations (46a) and (46b) suggest that the transmission line can be described by the lumped equivalent two-port of Thévenin type shown in Fig. 3 (e.g., Ref. [1]). Each port of the finite-length transmission line behaves as a resistor of resistance Z_c connected in series to a voltage source. It is a generalization of the lumped equivalent one-port for a semi-infinite transmission line, which is commonly used in the literature (e.g., Ref. [4]). However, unlike the semi-infinite case, for finite-length transmission lines, the voltage sources are not independent: they are controlled by the state equations (47a) and (47b), which are linear algebraic equations with one delay. A semi-infinite transmission line is equivalent to a resistor of resistance Z_c connected in series to an independent source with voltage $\hat{v}_{\rightarrow}^{(0)}$ or $\hat{v}_{\leftarrow}^{(0)}$, which are completely determined by the initial conditions.

The equivalent two-port of Thévenin type can be converted in the equivalent two-port of Norton type where each port consists of a resistor with resistance Z_c connected in parallel to a controlled current.

C. Equivalent lumped network and reduced equations of motion

The network consisting of a finite-length transmission line capacitively coupled to two lumped circuits $\mathcal{B}'$ and $\mathcal{B}''$ can be described by the equivalent lumped network with delay shown in Fig. 4. The left lumped circuit is governed by the system of reduced Heisenberg equations

$$\dot{\hat{\mathbf{\Phi}}}' = [\mathbf{A}']\hat{\mathbf{Q}}' + C_p'\mathbf{p}'\hat{V}_0', \tag{48a}$$

$$\dot{\hat{\mathbf{Q}}}' = -\mathbf{f}'(\hat{\mathbf{\Phi}}'), \tag{48b}$$

$$\dot{\hat{V}}_0' + \frac{1}{\tau'}\hat{V}_0' = -\mathbf{p}'^{\intercal}\mathbf{f}'(\hat{\mathbf{\Phi}}') + \frac{2}{\tau'}\hat{v}_{\leftarrow}(t), \tag{48c}$$

$$\hat{v}_{\leftarrow}(t + T) = \hat{V}_0''(t) - \hat{v}_{\rightarrow}(t), \tag{48d}$$

where $[\mathbf{A}'] = [\mathbf{C}_b']^{-1} - [\mathbf{B}']$, $[\mathbf{B}'] = C_p'\mathbf{p}'\mathbf{p}'^{\intercal}$, $\mathbf{f}'(\hat{\mathbf{\Phi}}') = \frac{\partial U_b'}{\partial \hat{\mathbf{\Phi}}'}$, and $\tau' = Z_c C_p'$. The right lumped circuit is governed by the system of reduced Heisenberg equations

$$\dot{\hat{\mathbf{\Phi}}}'' = [\mathbf{A}'']\hat{\mathbf{Q}}'' + C_p''\mathbf{p}''\hat{V}_0'', \tag{49a}$$

$$\dot{\hat{\mathbf{Q}}}'' = -\mathbf{f}''(\hat{\mathbf{\Phi}}''), \tag{49b}$$

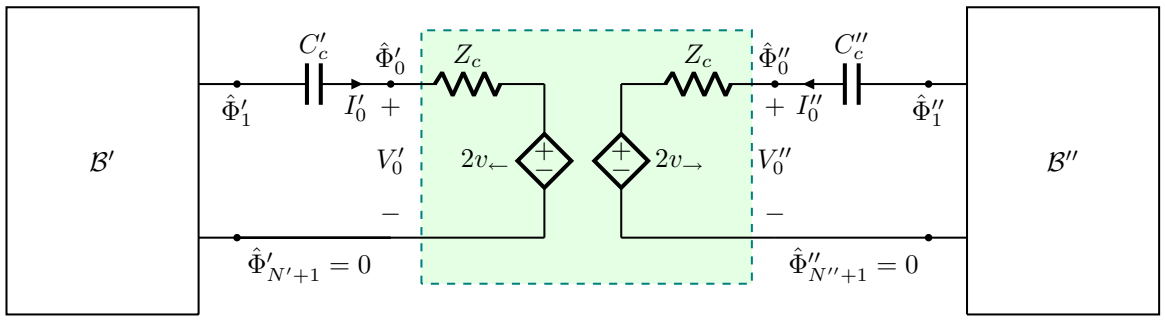

FIG. 4. Equivalent lumped network with delay for the finite-length transmission line capacitively coupled to the lumped circuits $\mathcal{B}'$ and $\mathcal{B}''$ shown in Fig. 2.

$$\dot{\hat{V}}''_0 + \frac{1}{\tau''}\hat{V}''_0 = -\mathbf{p}''^{\intercal}\mathbf{f}''(\hat{\mathbf{\Phi}}'') + \frac{2}{\tau''}\hat{v}_{\rightarrow}, \tag{49c}$$

$$\hat{v}_{\rightarrow}(t+T) = \hat{V}'_0(t) - \hat{v}_{\leftarrow}(t), \tag{49d}$$

where $[\mathbf{A}''] = [\mathbf{C}''_b]^{-1} - [\mathbf{B}'']$, $[\mathbf{B}''] = C''_p\mathbf{p}''\mathbf{p}''^{\intercal}$, $\mathbf{f}''(\hat{\mathbf{\Phi}}'') = \frac{\partial U''_b}{\partial \hat{\mathbf{\Phi}}''}$, and $\tau'' = Z_c C''_p$. The operator $\hat{V}'_0$ in the Schrödinger picture is given by $\hat{V}'^{(S)}_0 = \mathbf{p}'^{\intercal}\hat{\mathbf{Q}}'^{(S)} + \frac{1}{C'_p}\hat{Q}'^{(S)}_0$; the expression of $\hat{V}''^{(S)}_0$ is analogous. The system of Eqs. (48a)–(48d) and (49a)–(49d) are coupled through the Eqs. (48d) and (49d), which govern the controlled voltage sources.

The control laws of the voltage sources are linear algebraic equations with one delay. In the time interval $[iT, (i+1)T]$ with $i \geqslant 1$, the state operators $\hat{v}_{\rightarrow}(t)$ and $\hat{v}_{\leftarrow}(t)$ depend, respectively, only on the pair $\hat{v}_{\leftarrow}(t-T)$, $\hat{V}'_0(t-T)$ and the pair $\hat{v}_{\rightarrow}(t-T)$, $\hat{V}''_0(t-T)$ [for $0 < t < T$, $\hat{v}_{\rightarrow}(t)$ and $\hat{v}_{\leftarrow}(t)$ are given by the initial conditions (42)]. This characteristic enables us to treat the controlled sources as independent voltage sources if the problem is solved iteratively. Therefore, we can analyze systems consisting of transmission lines and lumped circuits iteratively, where at each step of the iteration we have to solve a reduced equivalent circuit composed only of lumped elements.

The operators $\hat{\mathbf{\Phi}}'^{(S)}$, $\hat{\mathbf{Q}}'^{(S)}$, $\hat{V}'^{(S)}_0$, $\hat{\mathbf{\Phi}}''^{(S)}$, $\hat{\mathbf{Q}}''^{(S)}$, $\hat{V}''^{(S)}_0$, $\hat{v}_{\leftarrow}(t)$, and $\hat{v}_{\rightarrow}(t)$ supplied by the two controlled voltage sources for $0 < t < T$ determine the time evolution of the observables. Once the generic observable is determined at time t, its statistics can be evaluated from the knowledge of the initial state of the transmission line and the lumped circuits.

D. Input-output formalism

The system of Eqs. (48) and (49) can be put in a quantum Langevin-like form by using the input-output formalism introduced for a semi-infinite transmission line coupled to a lumped circuit (e.g., Refs. [4,25]). The operator $\hat{v}_{\leftarrow}(t)$ is equal to the backward voltage wave operator at $x = 0$. It acts as the input operator for the lumped circuit $\mathcal{B}'$ connected to the left end of the line. Analogously, the operator $\hat{v}_{\rightarrow}(t)$, which is equal to the forward voltage wave operator at $x = d$, acts as the input operator for the lumped circuit $\mathcal{B}''$ connected to the right end. Therefore, we introduce the input operators $\hat{v}'_{\text{in}}(t)$ and $\hat{v}''_{\text{in}}(t)$ defined as $\hat{v}'_{\text{in}}(t) \equiv \hat{v}_{\leftarrow}(t)$ and $\hat{v}''_{\text{in}}(t) \equiv \hat{v}_{\rightarrow}(t)$. Within this formalism, the forward voltage wave operator at $x = 0$ acts as the outgoing voltage operator from the lumped circuit $\mathcal{B}'$, $\hat{v}'_{\text{out}}(t)$; analogously, the backward voltage wave operator at $x = d$ acts as the outgoing operator from the lumped circuit $\mathcal{B}''$, $\hat{v}''_{\text{out}}(t)$. From these definitions we have the following:

$$\hat{v}'_{\text{out}}(t) = \hat{V}'_0(t) - \hat{v}'_{\text{in}}(t), \tag{50a}$$

$$\hat{v}''_{\text{out}}(t) = \hat{V}''_0(t) - \hat{v}''_{\text{in}}(t). \tag{50b}$$

Unlike the semi-infinite transmission line, both input operators are determined by the initial conditions of the transmission line only for $0 < t < T$: for $t > T$ they are unknown and their evolution is governed by the system of equations (47a) and (47b). It is immediate that for $t > T$

$$\hat{v}'_{\text{in}}(t) = \hat{v}''_{\text{out}}(t-T), \tag{51a}$$

$$\hat{v}''_{\text{in}}(t) = \hat{v}'_{\text{out}}(t-T). \tag{51b}$$

From Eqs. (48b), (48c), (49b), and (49c) we obtain

$$\hat{V}'_0 = \mathbf{p}'^{\intercal} g' * \dot{\hat{\mathbf{Q}}}' + \frac{2}{\tau'} g' * \hat{v}'_{\text{in}} + \hat{V}'^{(S)}_0 g', \tag{52a}$$

$$\hat{V}''_0 = \mathbf{p}''^{\intercal} g'' * \dot{\hat{\mathbf{Q}}}'' + \frac{2}{\tau''} g'' * \hat{v}''_{\text{in}} + \hat{V}''^{(S)}_0 g'', \tag{52b}$$

where $g'(t) = u(t)e^{-t/\tau'}$, $g''(t) = u(t)e^{-t/\tau''}$, and the symbol $*$ denotes the time convolution product over the interval $[0, t]$. Therefore, the system of Eqs. (48) and (49) can be further reduced to

$$\dot{\hat{\mathbf{\Phi}}}' = \frac{1}{i\hbar}[\hat{\mathbf{\Phi}}', \hat{H}'_{\text{cir}}] + [\mathbf{B}']g' * \dot{\hat{\mathbf{Q}}}' + C'_p\mathbf{p}'\left(\frac{2}{\tau'} g' * \hat{v}'_{\text{in}} + g'\hat{V}'^{(S)}_0\right), \tag{53a}$$

$$\dot{\hat{\mathbf{Q}}}' = \frac{1}{i\hbar}[\hat{\mathbf{Q}}', \hat{H}'_{\text{cir}}], \tag{53b}$$

and

$$\dot{\hat{\mathbf{\Phi}}}'' = \frac{1}{i\hbar}[\hat{\mathbf{\Phi}}'', \hat{H}''_{\text{cir}}] + [\mathbf{B}'']g'' * \dot{\hat{\mathbf{Q}}}'' + C''_p\mathbf{p}''\left(\frac{2}{\tau''} g'' * \hat{v}''_{\text{in}} + g''\hat{V}''^{(S)}_0\right), \tag{54a}$$

$$\dot{\hat{\mathbf{Q}}}'' = \frac{1}{i\hbar}[\hat{\mathbf{Q}}'', \hat{H}''_{\text{cir}}], \tag{54b}$$

where $\hat{H}'_{\text{cir}} = \frac{1}{2}\hat{\mathbf{Q}}'^{\intercal}[\mathbf{A}']\hat{\mathbf{Q}}' + U'_c(\hat{\mathbf{\Phi}}')$ and $\hat{H}''_{\text{cir}} = \frac{1}{2}\hat{\mathbf{Q}}''^{\intercal}[\mathbf{A}'']\hat{\mathbf{Q}}'' + U''_c(\hat{\mathbf{\Phi}}'')$.

The system of Eqs. (53a) and (53b) are the equations of the lumped circuit $\mathcal{B}'$ in the quantum Langevin-like form, and the system of Eqs. (54a) and (54b) are the equations of the lumped circuit $\mathcal{B}''$ (e.g., Ref. [25]). These equations coincide with the those governing a circuit connected to a semi-infinite line, but unlike what happens for a semi-infinite line, the input operators $\hat{v}'_{\rm in}$ and $\hat{v}''_{\rm in}$ are unknown for $t > T$. The Eqs. (53a) and (53b) and the Eqs. (54a) and (54b) are coupled through the Eqs. (50) and (51), which account for the multireflection at the line ends. However, the overall system is closed, differently from the case of a semi-infinite transmission line.

When $1/\tau'$ and $1/\tau''$ are significantly higher than the highest characteristic frequencies of the system, the memory functions $g'(t)$ and $g''(t)$ go to zero on time scales that are much lower than the times over which $\dot{\hat{\mathbf{Q}}}'$ and $\dot{\hat{\mathbf{Q}}}''$ change. Then, we can replace $g'(t)$ with $\tau'\delta(t)$ and $g''(t)$ with $\tau''\delta(t)$ where $\delta(t)$ is the Dirac delta function (first Markov approximation). Furthermore, for t not close to 0 we can drop $g'(t)\hat{V}_0'^{(S)}$ and $g''(t)\hat{V}_0''^{(S)}$. In this approximation, Eqs. (52) reduce to

$$\hat{V}'_0 = \tau' \mathbf{p}'^{\intercal} \dot{\hat{\mathbf{Q}}}' + 2\hat{v}'_{\rm in}, \tag{55a}$$

$$\hat{V}''_0 = \tau'' \mathbf{p}''^{\intercal} \dot{\hat{\mathbf{Q}}}'' + 2\hat{v}''_{\rm in}, \tag{55b}$$

Eq. (53a) reduces to

$$\dot{\hat{\mathbf{\Phi}}}' = \frac{1}{i\hbar}[\hat{\mathbf{\Phi}}', \hat{H}'_{\rm cir}] + \tau'[\mathbf{B}']\dot{\hat{\mathbf{Q}}}' + 2C'_p \mathbf{p}' \hat{v}'_{\rm in}, \tag{56}$$

and Eq. (54a) reduces to

$$\dot{\hat{\mathbf{\Phi}}}'' = \frac{1}{i\hbar}[\hat{\mathbf{\Phi}}'', \hat{H}''_{\rm cir}] + \tau''[\mathbf{B}']\dot{\hat{\mathbf{Q}}}'' + 2C''_p \mathbf{p}'' \hat{v}''_{\rm in}. \tag{57}$$

Equations (56) and (57) are, respectively, the equations of motion of the lumped circuits $\mathcal{B}'$ and $\mathcal{B}''$ in quantum Langevin-like form, in the Markovian approximation. Equations (56) and (57) are consistent with the ones found in Refs. [14,27].

V. AN APPLICATION

In this section, we examine the network depicted in Fig. 2, when the lumped circuit $\mathcal{B}'$ is made of a linear capacitor C'_r connected in parallel to an inductor with energy U'_b, and the lumped circuit $\mathcal{B}''$ is made of a linear capacitor C''_r connected in parallel to an inductor with energy U''_b.

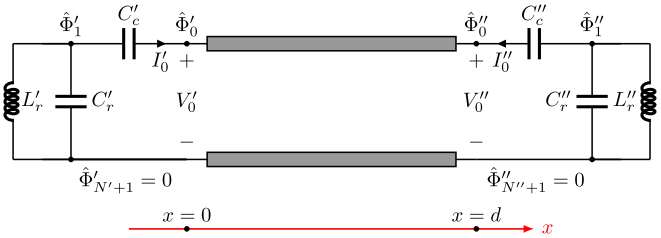

FIG. 5. A finite-length transmission line capacitively coupled to two linear LC circuits.

Eliminating the observables $\hat{Q}'_1$ and $\hat{Q}''_1$, the system of Eqs. (48) reduces to

$$\ddot{\hat{\Phi}}'_1 + \frac{1}{(C'_r + C'_c)} f'(\hat{\Phi}'_1) = \frac{C'_p}{C'_r}\dot{\hat{V}}'_0, \tag{58a}$$

$$\dot{\hat{V}}'_0 + \frac{1}{\tau'}\hat{V}'_0 = -\frac{1}{C'_r} f'(\hat{\Phi}'_1) + \frac{2}{\tau'}\hat{v}_{\leftarrow}, \tag{58b}$$

$$\hat{v}_{\leftarrow}(t+T) = \hat{V}''_0(t) - \hat{v}_{\rightarrow}(t), \tag{58c}$$

and the system of Eqs. (49) reduces to

$$\ddot{\hat{\Phi}}''_1 + \frac{1}{(C''_r + C''_c)} f''(\hat{\Phi}''_1) = \frac{C''_p}{C''_r}\dot{\hat{V}}''_0, \tag{59a}$$

$$\dot{\hat{V}}''_0 + \frac{1}{\tau''}\hat{V}''_0 = -\frac{1}{C''_r} f''(\hat{\Phi}''_1) + \frac{2}{\tau''}\hat{v}_{\rightarrow}, \tag{59b}$$

$$\hat{v}_{\rightarrow}(t+T) = \hat{V}'_0(t) - \hat{v}_{\leftarrow}(t), \tag{59c}$$

where $C'_p = C'_c C'_r/(C'_c + C'_r)$, $C''_p = C''_c C''_r/(C''_c + C''_r)$, $f'(\hat{\Phi}'_1) = \frac{\partial U'_b}{\partial \hat{\Phi}'_1}$, and $f''(\hat{\Phi}''_1) = \frac{\partial U''_b}{\partial \hat{\Phi}''_1}$. The operator $\hat{V}'_0$ in the Schrödinger picture is given by $\hat{V}_0'^{(S)} = \frac{1}{C'_r}\hat{Q}_1'^{(S)} + \frac{1}{C'_p}\hat{Q}_0'^{(S)}$; the expression of $\hat{V}_0''^{(S)}$ is analogous.

In the case shown in Fig. 5 where the inductors are linear, and therefore $U' = \frac{1}{2L'_r}(\hat{\Phi}'_1)^2$ and $U'' = \frac{1}{2L''_r}(\hat{\Phi}''_1)^2$, the system of equations (58) and (59) can be solved analytically by applying the Laplace transform. In the Laplace domain, we obtain:

$$\mathbf{M}(s)\hat{\mathbf{U}}(s) = \hat{\mathbf{F}}(s), \tag{60}$$

where $\hat{\mathbf{U}}(s) = |\hat{\Phi}_1'^{\rm L}(s), \hat{V}_0'^{\rm L}(s), \hat{\Phi}_1''^{\rm L}(s), \hat{V}_0''^{\rm L}(s)|^{\intercal}$, $\hat{\Phi}_1'^{\rm L}(s)$, $\hat{V}_0'^{\rm L}(s)$, $\hat{\Phi}_1''^{\rm L}(s)$, and $\hat{V}_0''^{\rm L}(s)$ are, respectively, the Laplace transforms of $\hat{\Phi}'_1(t)$, $\hat{V}'_0(t)$, $\hat{\Phi}''_1(t)$, and $\hat{V}''_0(t)$; the matrix $\mathbf{M}(s)$ is given by

$$\mathbf{M} = \begin{pmatrix} \left[s^2 + \frac{1}{L'_r(C'_c+C'_r)}\right] & -s\frac{C'_p}{C'_r} & 0 & 0 \\ \frac{1}{L'_r C'_r} & \left[s + \frac{1}{\tau'}\coth(sT)\right] & 0 & -\frac{1}{\tau'}\frac{1}{\sinh(sT)} \\ 0 & 0 & \left[s^2 + \frac{1}{L''_r(C''_c+C''_r)}\right] & -s\frac{C''_p}{C''_r} \\ 0 & -\frac{1}{\tau''}\frac{1}{\sinh(sT)} & \frac{1}{L''_r C''_r} & \left[s + \frac{1}{\tau''}\coth(sT)\right] \end{pmatrix}; \tag{61}$$

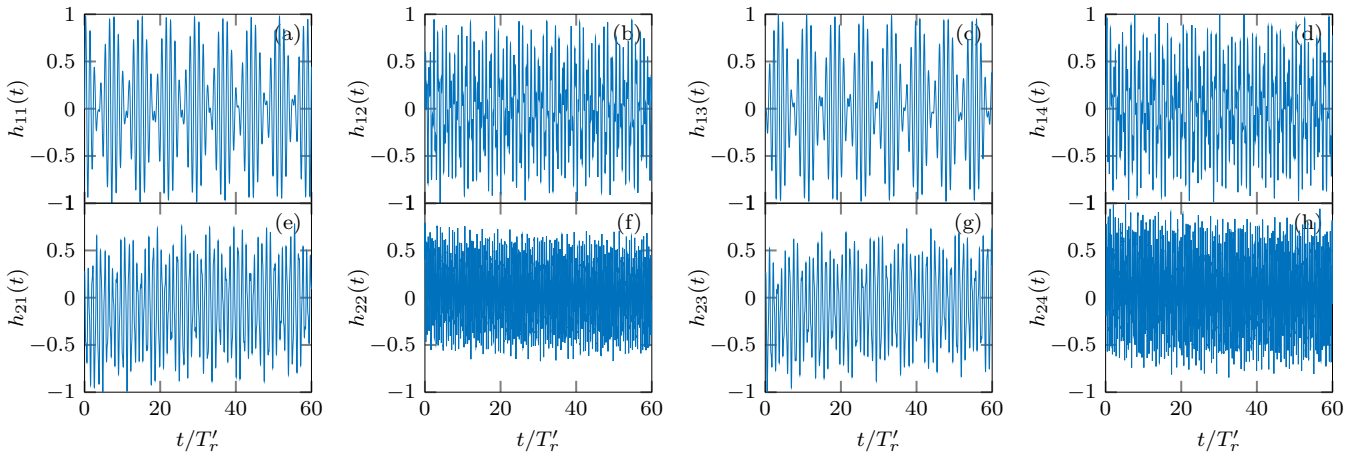

FIG. 6. Selected entries of the impulse response matrix $\mathbf{h}(t)$ of a finite-length transmission line capacitively coupled to two identical LC circuits with parameters $g' = 0.3$ $\alpha' = 2$, and $\gamma' = 2\pi \times 0.1$. Each impulse response is normalized to its maximum absolute value.

the entries of the known operator $\hat{\mathbf{F}}(s) = |\hat{F}_1'(s), \hat{F}_2'(s), \hat{F}_1''(s), \hat{F}_2''(s)|^\intercal$ are given by

$$\hat{F}_1'(s) = \dot{\hat{\Phi}}_1'(0) + s\hat{\Phi}_1'(0) - \frac{C_p'}{C_r'}\hat{V}_0'(0), \tag{62a}$$

$$\hat{F}_2'(s) = \hat{V}_0'(0) - \frac{1}{\tau'}\frac{\hat{V}_{\rightarrow}^{(0)}(s) - e^{sT}\hat{V}_{\leftarrow}^{(0)}(s)}{\sinh(sT)}, \tag{62b}$$

and

$$\hat{F}_1''(s) = \dot{\hat{\Phi}}_1''(0) + s\hat{\Phi}_1''(0) - \frac{C_p''}{C_r''}\hat{V}_0''(0), \tag{63a}$$

$$\hat{F}_2''(s) = \hat{V}_0''(0) + \frac{1}{\tau''}\frac{e^{sT}\hat{V}_{\rightarrow}^{(0)}(s) - \hat{V}_{\leftarrow}^{(0)}(s)}{\sinh(sT)}, \tag{63b}$$

where

$$\hat{V}_{\rightarrow}^{(0)}(s) = \int_0^T \hat{v}_{\rightarrow}^{(0)}(t)e^{st}dt, \tag{64a}$$

$$\hat{V}_{\leftarrow}^{(0)}(s) = \int_0^T \hat{v}_{\leftarrow}^{(0)}(t)e^{st}dt, \tag{64b}$$

take into account the contributions of the initial conditions $\hat{v}_{\rightarrow}(t) = \hat{v}_{\rightarrow}^{(0)}(t)$ and $\hat{v}_{\leftarrow}(t) = \hat{v}_{\leftarrow}^{(0)}(t)$ for $0 < t < T$.

From Eq. (60) we obtain $\hat{\mathbf{u}}(t) = \mathbf{h}(t) * \hat{\mathbf{f}}(t)$ where $\hat{\mathbf{u}}(t) = |\hat{\Phi}_1'(t), \hat{V}_0'(t), \hat{\Phi}_1''(t), \hat{V}_0''(t)|^\intercal$, $\hat{\mathbf{f}}(t)$ is the inverse Laplace transform of $\hat{\mathbf{F}}(s)$, and the impulse response matrix $\mathbf{h}(t)$ is the inverse Laplace transform of $\mathbf{H}(s) = \mathbf{M}^{-1}(s)$. Once $\hat{V}_0'(t)$ and $\hat{V}_0''(t)$ have been evaluated, we can compute $\hat{v}_{\leftarrow}(t)$ and $\hat{v}_{\rightarrow}(t)$ for $T < t$ using Eqs. (47a) and (47b) with the initial conditions $\hat{v}_{\rightarrow}(t) = \hat{v}_{\rightarrow}^{(0)}(t)$ and $\hat{v}_{\leftarrow}(t) = \hat{v}_{\leftarrow}^{(0)}(t)$ for $0 < t < T$.

The poles of $\mathbf{H}(s)$ correspond to the zeros of the determinant of the matrix $\mathbf{M}(s)$, whose expression is given in Appendix A: they are associated with the natural modes of the network. Unlike the semi-infinite transmission line scenario discussed in Ref. [29], the matrix $\mathbf{H}(s)$ has an infinite number of discrete poles, all located on the imaginary axis of the complex plane. This discreteness arises due to the finite length of the line, and the infinity is a consequence of multireflections at the line ends. The real part of the poles is equal to zero because the entire network is a closed conservative system.

The matrix $\mathbf{h}(t)$ is the classical matrix impulse response of the network. The terms $h_{11}(t)$ and $h_{13}(t)$ are, respectively, the responses of the flux $\Phi_1'(t)$ when the inductor L_r' and the inductor L_r'' are instantaneously charged by an impulsive voltage source with unitary amplitude; $h_{21}(t)$ and $h_{22}(t)$ are the response of $V_0'(t)$ when the inductor L_r' is instantaneously charged by an impulsive voltage source with unitary amplitude, and the backward voltage wave at $x = 0$ is a Dirac pulse with amplitude equal to 0.5.

We now investigate the scenario in which the transmission line is connected to two identical LC circuits, with equal values for the inductances, i.e., $L_r' = L_r''$, and capacitances, i.e., $C_r' = C_r''$, through two identical capacitors ($C_c' = C_c''$). In Appendix A, we study the natural frequency of this network. The entries of $\mathbf{h}(t)$ are numerically evaluated using the IFFT algorithm. In Figs. 6–8, we show the time evolution of the entries of the first two rows of $\mathbf{h}(t)$ for $\gamma' = 0.1 \times 2\pi$, $\gamma' = 1 \times 2\pi$, and $\gamma' = 10 \times 2\pi$, where $\gamma' = T/T_r'$ and $T_r' = 2\pi/\sqrt{L_r'C_r'}$; we have fixed $g' = 0.3$ and $\alpha' = 2$, where $g' = C_c'/(C_r' + C_c')$, $\alpha' = Z_c'/Z_r'$ and $Z_r' = \sqrt{L_r'/C_r'}$. Due to the left-right symmetry of the network, by reversing the temporal patterns of the elements in the first and second rows, you obtain the temporal patterns of the elements in the third and fourth rows.

In each time interval $[iT, (i+1)T]$ with $i = 0, 1, \ldots$ the LC circuit on the left-hand side (right-hand side) of the network behaves as if it were effectively capacitively coupled to a semi-infinite line with characteristic impedance Z_c: the backward voltage (input) operator at $x = 0$ (the forward voltage operator at $x = d$) is determined either by the initial conditions of the transmission line or by the reflections at $x = d$ (at $x = 0$) due to the interaction with the other LC circuit. The time evolution of the circuit on the left-hand side depends on several characteristic times: the oscillation period T_r' of the LC circuit, the decay time of the oscillation that we would have if the LC circuit were capacitively coupled to a semi-infinite line, and the delay time of the line T. Figures 6(a) and 6(c) show, respectively, $h_{11}(t)$ and $h_{13}(t)$ versus t/T_r' for $\gamma' = 0.1 \times 2\pi$. In this scenario, the delay time T is one-tenth the LC oscillation period T_r'. The effects of the delay are negligible, and the two LC circuits behave as they interact almost instantaneously. In particular, $h_{11}(t)$ and $h_{13}(t)$

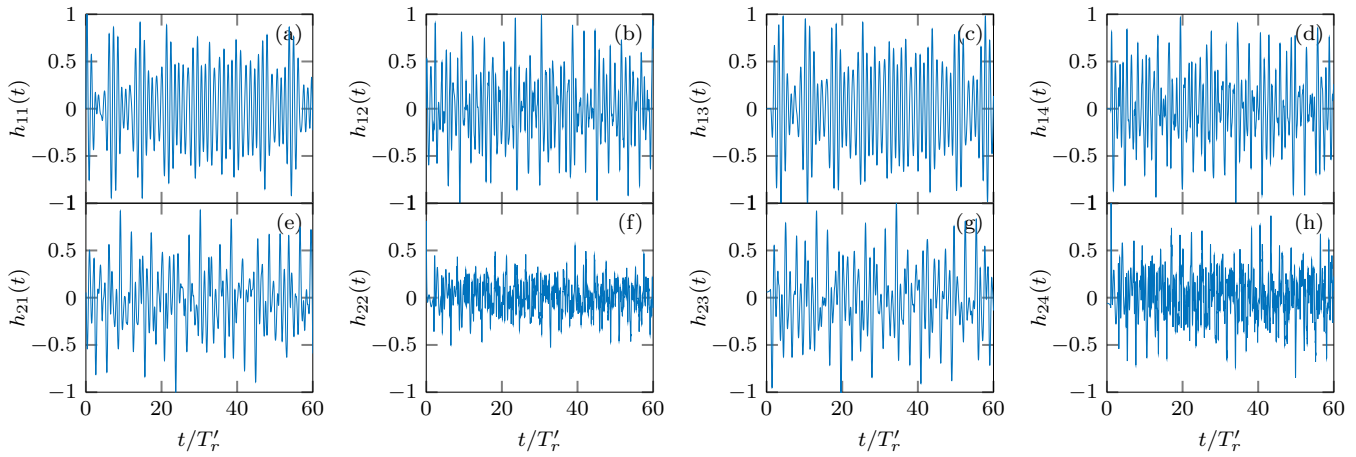

FIG. 7. Selected entries of the impulse response matrix $\mathbf{h}(t)$ of a finite-length transmission line capacitively coupled to two identical LC circuits with parameters $g' = 0.3$ $\alpha' = 2$, and $\gamma' = 2\pi \times 1$. Each impulse response is normalized to its maximum absolute value.

show a beating between the fundamental frequency, which is almost equal to $\omega_r' = 1/\sqrt{L_r' C_r'}$, and the envelope frequency $(\omega_2 - \omega_1)/2$, where ω_1 and ω_2 are the natural frequencies of the first two modes of the network (see Appendix A). Figures 7(a) and 7(c) show the same impulse responses for $\gamma' = 1 \times 2\pi$. In this case, the delay time is equal to the oscillation period of each LC circuit. Despite the increase in delay T, its effects remain of little importance. In this case, $h_{11}(t)$ and $h_{13}(t)$ show a beating due to the interference between the second and third modes (see Appendix A). Moreover, a low-frequency modulation arises due to the fundamental mode. Figures 8(a) and 8(c) show the same impulse responses for $\gamma' = 10 \times 2\pi$. In this case, the delay time T is ten times the LC oscillation period T_r', and it is also greater than the decay time. As a consequence, the effects of the delay are important. Effectively, the LC circuit on the left behaves as if it were capacitively connected to a semi-infinite transmission line for $0 < t/T_r' < 10$ with a backward voltage wave at $x = 0$ equal to zero, as shown in Fig. 8(a). At $t/T_r' = 20$ the backward voltage wave due to the reflection at $x = d$ of the forward voltage wave generated at $x = 0$ starts to drive the LC circuit on the left, and so on. Figure 8(c) shows a similar behavior. Similar considerations apply to the LC circuit on the right.

Finally, we briefly discuss the behavior of the other entries in the impulse response matrix. For $\gamma' = 0.1 \times 2\pi$ and $\gamma' = 1 \times 2\pi$, the behavior of $h_{12}(t)$, $h_{14}(t)$, $h_{21}(t)$, $h_{22}(t)$, $h_{23}(t)$, and $h_{24}(t)$ reflect the influence of high-frequency modes. For $\gamma' = 10 \times 2\pi$ the impact of the line delay becomes pronounced, though the contribution of higher-order modes appears less evident.

VI. CONCLUSIONS

We have introduced an equivalent two-port model to analyze finite-length transmission lines within quantum circuit electrodynamics. This model, framed in the Heisenberg picture, consists of a series of a resistor and a controlled source with delay at each port. We apply this model to a transmission line capacitively coupled to two lumped circuits, and derive a reduced system of Heisenberg equations that governs the lumped circuits. We then recast the reduced equations of each lumped circuit in a quantum Langevin-like form. These equations are coupled due to multireflection at the line ends, and together describe the evolution of a closed system. Due to the time delay T, introduced by the transmission line, the dynamic of the lumped circuit on the first port influences the evolution

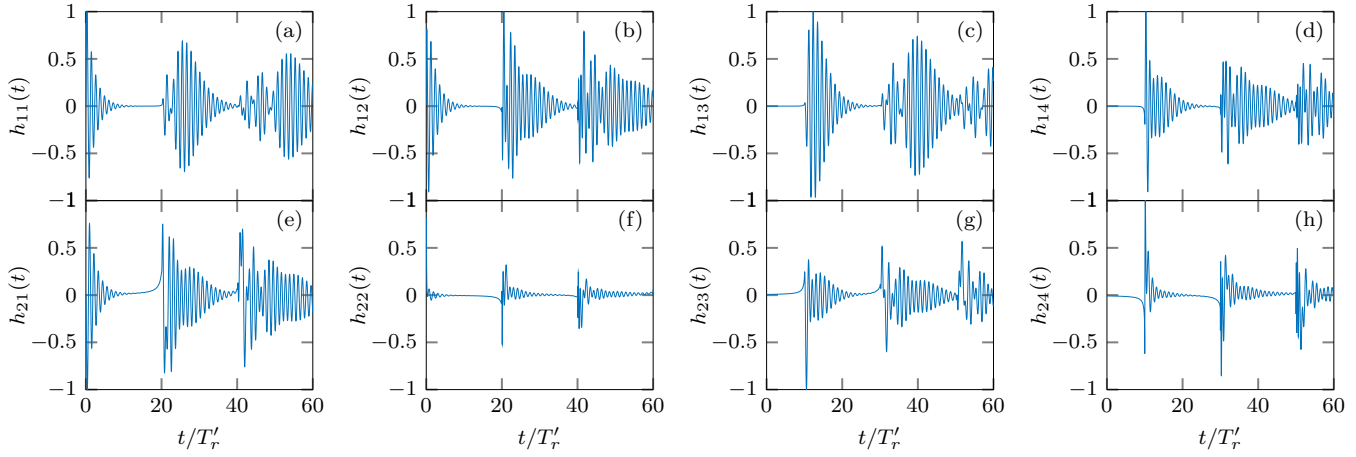

FIG. 8. Selected entries of the impulse response matrix $\mathbf{h}(t)$ of a finite-length transmission line capacitively coupled to two identical LC circuits with parameters $g' = 0.3$ $\alpha' = 2$, and $\gamma' = 2\pi \times 10$. Each impulse response is normalized to its maximum absolute value.

of the lumped circuit connected to the second port after a time T, and vice versa.

We demonstrated the applicability of our model by solving the reduced system of Heisenberg equations in a linear scenario admitting an analytical solution, which consists of a finite-length transmission line capacitively coupled to two LC circuits. Now, we briefly discuss the application of this model to nonlinear circuits. Consider two nonlinear lumped circuits coupled by a transmission line, each comprising a parallel configuration of a capacitor and a nonlinear inductor. This configuration holds significant relevance for current research in quantum circuit electrodynamics [7–13]. The overall system is described by Eqs. (58)–(59). The nonlinear inductors can be, for example, two Josephson junctions with $U_b' = -E_J' \cos(2\pi \hat{\Phi}_1'/\Phi_0)$ and $U_b'' = -E_J'' \cos(2\pi \hat{\Phi}_1''/\Phi_0)$, where Φ_0 is the flux quantum. In this case, Eqs. (58)–(59) have to be solved numerically as outlined below. The time derivatives of the operators $\hat{\Phi}'$, $\hat{\Phi}''$, $\hat{V}_0'$, and $\hat{V}_0''$ can be discretized by finite differences or finite elements [31,32]. The operators can be represented as matrices by selecting a suitable basis for the state space. The resulting discrete equations for the matrix entries form a system of nonlinear equations. This system can be vectorized and solved using standard methods for nonlinear equations, such as the Newton's method. The main computational challenge arises from the potentially large dimension of the state space of the overall system, which is given by the tensor product of the state space of the transmission line, which enters through the initial conditions (42) on the line operators, and the state space of two lumped parts of the system. This issue is even more pronounced when the line is described by using alternative approaches, where the degrees of freedom of the line are represented either in terms of modes or through several lumped LC elements, because in these cases the accuracy of the description of the propagation along the line depends on the dimension of the discretized state space of the line. This problem is particularly critical in scenarios where the transmission line length exceeds the operational wavelength. In contrast, our formulation enables a reduction in computational time, for a specified accuracy level, by analytically incorporating the contribution of the line.

In conclusion, our model not only simplifies the study of finite-length transmission lines in quantum circuits but also paves the way for exploring more complex coupling configurations. It holds potential for broader applications, including scenarios involving multiconductor transmission lines and various combinations of capacitive and inductive coupling between the lines and the lumped circuits. This flexibility and generality make our approach a valuable tool for advancing research in quantum circuit electrodynamics.

ACKNOWLEDGMENTS

This work was supported by Ministero dell'Università e della Ricerca under the PNRR Projects No. PE0000023-NQSTI and No. CN00000013-ICSC.

APPENDIX: NATURAL FREQUENCIES

The expression of the determinant of the matrix $\mathbf{M}(s)$ given by (61) is

$$
\begin{aligned}
p(s) = -&\left[\left(\frac{s}{\omega_r'}\right)^2 + (1-g')\right]\left[\left(\frac{s}{\omega_r''}\right)^2 + (1-g'')\right]\left\{\left[\frac{s}{\omega_r'} + \frac{1}{\alpha' g'}\coth\left(\frac{s}{\omega_r'}\gamma'\right)\right]\left[\frac{s}{\omega_r''} + \frac{1}{\alpha'' g''}\coth\left(\frac{s}{\omega_r''}\gamma''\right)\right]\right. \\
&\left. - \frac{1}{\alpha' g'}\frac{1}{\alpha'' g''}\frac{1}{\sinh\left(\frac{s}{\omega_r'}\gamma'\right)}\frac{1}{\sinh\left(\frac{s}{\omega_r''}\gamma''\right)}\right\} - \left[\left(\frac{s}{\omega_r'}\right)^2 + (1-g')\right]\left[\frac{s}{\omega_r'} + \frac{1}{\alpha' g'}\coth\left(\frac{s}{\omega_r'}\gamma'\right)\right]g''\frac{s}{\omega_r''} \\
&- \left[\left(\frac{s}{\omega_r''}\right)^2 + (1-g'')\right]\left[\frac{s}{\omega_r''} + \frac{1}{\alpha'' g''}\coth\left(\frac{s}{\omega_r''}\gamma''\right)\right]g'\frac{s}{\omega_r'} - g'g''\frac{s^2}{\omega_r'\omega_r''},
\end{aligned}
\tag{A1}
$$

where $\omega_r' = 1/\sqrt{L_r' C_r'}$, $g' = C_c'/(C_r' + C_c')$, $\alpha' = Z_c'/Z_r'$, $Z_r' = \sqrt{L_r'/C_r'}$, $T_r' = 2\pi/\omega_r'$, $\gamma' = T/T_r'$, and $\omega_r'' = 1/\sqrt{L_r'' C_r''}$, $g'' = C_c''/(C_r'' + C_c'')$, $\alpha'' = Z_c''/Z_r''$, $Z_r'' = \sqrt{L_r''/C_r''}$, $T_r'' = 2\pi/\omega_r''$, $\gamma'' = T/T_r''$. The zeros of $p(s)$ correspond to the poles of the matrix $\mathbf{H}(s) = \mathbf{M}^{-1}(s)$, and are associated with the natural modes of the network. The set of poles of $\mathbf{H}(s)$ is discrete. They are all located on the imaginary axis because the system is conservative [$s = 0$ is a zero of $p(s)$]. By substituting $s = i\omega$ into the expression of $p(s)$ we obtain a real function of the real variable ω, which is a transcendental function. The values of ω for which $p(i\omega) = 0$ are the natural frequencies of the modes supported by the network and, consequently, its resonance frequencies. They can be evaluated numerically by using a root-finding algorithm.

We analyze the scenario in which the two LC circuits at the ends of the line and the two coupling capacitors are equal. In this case, the resonance frequencies can be evaluated by the graphical method. Equation $p(i\omega) = 0$ reduces to

$$
G(\tilde{\omega}; g', \alpha') = \tan\left(\tilde{\omega}\gamma'\right), \tag{A2}
$$

where

$$
G = -2\frac{\frac{\tilde{\omega}^2 - (1-g')}{\tilde{\omega}\alpha' g'(\tilde{\omega}^2 - 1)}}{\left[\frac{\tilde{\omega}^2 - (1-g')}{\tilde{\omega}\alpha' g'(\tilde{\omega}^2 - 1)}\right]^2 - 1}, \tag{A3}
$$

and $\tilde{\omega} = \omega/\omega_r'$. The set of solutions of Eq. (A2) is discrete and infinite. We denote them by $\{\tilde{\omega}_n\}$, where the integer n runs from $-\infty$ to $+\infty$. Both the functions $G(\tilde{\omega}; g', \alpha')$ and $\tan(\tilde{\omega}\gamma')$ are odd in the variable $\tilde{\omega}$, hence $\tilde{\omega}_{-n} = -\tilde{\omega}_n$ for any $n > 0$, and $\tilde{\omega}_0 = 0$. Therefore, the unknowns reduce to

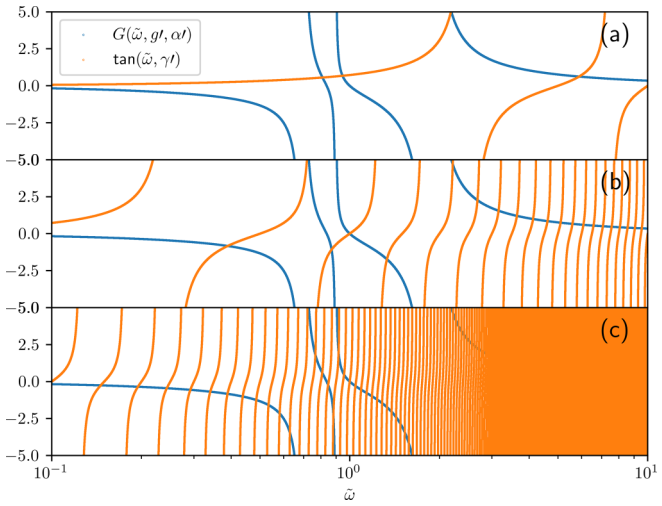

FIG. 9. The intersections between the blue and the orange curves give the normalized natural frequencies of the modes of a finite-length transmission line connected to two equal LC circuits ($L_r' = L_r''$ and $C_r' = C_r''$) through two equal capacitors ($C_c' = C_c''$), for $g' = 0.3$, $\alpha' = 2$ and (a) $\gamma' = 0.1 \times 2\pi$, (b) $\gamma' = 1 \times 2\pi$, (c) $\gamma' = 10 \times 2\pi$.

$\tilde{\omega}_1, \tilde{\omega}_2, \ldots, \tilde{\omega}_n, \ldots$, which are ordered in such a way $\tilde{\omega}_n < \tilde{\omega}_{n+1}$ for $n = 1, 2, \ldots$. In Fig. 9, we look for the intersections of the two functions $G(\tilde{\omega}; g', \alpha')$ and $\tan(\tilde{\omega}\gamma')$ for $\tilde{\omega}$ belonging to the interval (0.1,10). We assume $g' = 0.3$, $\alpha' = 2$, and different values of γ', namely $0.1 \times 2\pi$ in Fig. 9(a), 2π in Fig. 9(b), and $10 \times 2\pi$ in Fig. 9(c). The abscissas of the points where the two curves intersect are the positive solutions of Eq. (A2) in the interval (0.1,10). The number of positive solutions on the left of $\tilde{\omega} = 1$ is finite, while on the right it is infinite. In particular, we have $\tilde{\omega}_n \to n\pi/\gamma'$ as $n \to +\infty$ because $G \to 0$ for $\tilde{\omega} \to \infty$: these are the normalized natural frequencies of the transmission line when it is connected to two short circuits or to two open circuits. As the length of the line increases, the positive solutions shift to the left and some of them cross the value $\tilde{\omega} = 1$. As a consequence, the number of solutions belonging to the interval (0,1) also increases. Furthermore, the distance between contiguous solutions reduces. As $\gamma' \to \infty$ the set of solutions approaches a continuum that spans the interval $(0, \infty)$. In particular, we note that for $\gamma' = 0.1 \times 2\pi$ we have $\tilde{\omega}_1 < 1$ and $\tilde{\omega}_2 > 1$ with $(\tilde{\omega}_2 + \tilde{\omega}_1)/2 \approx 1$ and $(\tilde{\omega}_2 - \tilde{\omega}_1)/2 \ll 1$. For $\gamma' = 1 \times 2\pi$, we have $\tilde{\omega}_2 < 1$ and $\tilde{\omega}_3 > 1$ with $(\tilde{\omega}_3 + \tilde{\omega}_2)/2 \approx 1$ and $(\tilde{\omega}_3 - \tilde{\omega}_2)/2 \ll 1$, while $\tilde{\omega}_1$ is included between 0.3 and 0.4. Eventually, for $\gamma' = 10 \times 2\pi$, we have 18 positive solutions less than 1. We carried out several numerical experiments and we concluded that the qualitative properties of the solutions of Eq. (A2) are almost unaffected when the parameters g' and α' vary.

[1] G. Miano and A. Maffucci, *Transmission Lines and Lumped Circuits: Fundamentals and Applications*, 1st ed. (Academic Press, San Diego, 2001).

[2] M. H. Devoret and R. J. Schoelkopf, Superconducting circuits for quantum information: An outlook, Science **339**, 1169 (2013).

[3] A. Blais, A. L. Grimsmo, S. M. Girvin, and A. Wallraff, Circuit quantum electrodynamics, Rev. Mod. Phys. **93**, 025005 (2021).

[4] U. Vool and M. Devoret, Introduction to quantum electromagnetic circuits, Int. J. Circuit Theory Appl. **45**, 897 (2017).

[5] A. Ciani, D. P. DiVincenzo, and B. M. Terhal, Lecture notes on quantum electrical circuits, arXiv:2312.05329 [quant-ph].

[6] A. Parra-Rodriguez, E. Rico, E. Solano, and I. L. Egusquiza, Quantum networks in divergence-free circuit QED, Quantum Sci. Technol. **3**, 024012 (2018).

[7] P. Kurpiers, P. Magnard, T. Walter, B. Royer, M. Pechal, J. Heinsoo, Y. Salathe, A. Akin, S. Storz, J.-C. Besse, S. Gasparinetti, A. Blais, and A. Wallraff, Deterministic quantum state transfer and remote entanglement using microwave photons, Nature (London) **558**, 264 (2018).

[8] C. J. Axline, L. D. Burkhart, W. Pfaff, M. Zhang, K. Chou, P. Campagne-Ibarcq, P. Reinhold, L. Frunzio, S. M. Girvin, L. Jiang, M. H. Devoret, and R. J. Schoelkopf, On-demand quantum state transfer and entanglement between remote microwave cavity memories, Nat. Phys. **14**, 705 (2018).

[9] P. Magnard, S. Storz, P. Kurpiers, J. Schär, F. Marxer, J. Lütolf, T. Walter, J.-C. Besse, M. Gabureac, K. Reuer, A. Akin, B. Royer, A. Blais, and A. Wallraff, Microwave quantum link between superconducting circuits housed in spatially separated cryogenic systems, Phys. Rev. Lett. **125**, 260502 (2020).

[10] Y. Zhong, H.-S. Chang, A. Bienfait, Ã. Dumur, M.-H. Chou, C. R. Conner, J. Grebel, R. G. Povey, H. Yan, D. I. Schuster, and A. N. Cleland, Deterministic multi-qubit entanglement in a quantum network, Nature (London) **590**, 571 (2021).

[11] D. Awschalom, K. K. Berggren, H. Bernien, S. Bhave, L. D. Carr, P. Davids, S. E. Economou, D. Englund, A. Faraon, M. Fejer, S. Guha, M. V. Gustafsson, E. Hu, L. Jiang, J. Kim, B. Korzh, P. Kumar, P. G. Kwiat, M. Loncar, M. D. Lukin, D. A. B. Miller, C. Monroe, S. W. Nam, P. Narang, J. S. Orcutt, M. G. Raymer, A. H. Safavi-Naeini, M. Spiropulu, K. Srinivasan, S. Sun, J. Vuckovic, E. Waks, R. Walsworth, A. M. Weiner, and Z. Zhang, Development of quantum interconnects (QuICs) for next-generation information technologies, PRX Quantum **2**, 017002 (2021).

[12] B. Kannan, A. Almanakly, Y. Sung, A. Di Paolo, D. A. Rower, J. Braumüller, A. Melville, B. M. Niedzielski, A. Karamlou, K. Serniak, A. Vepsäläinen, M. E. Schwartz, J. L. Yoder, R. Winik, J. I.-J. Wang, T. P. Orlando, S. Gustavsson, J. A. Grover, and W. D. Oliver, On-demand directional microwave photon emission using waveguide quantum electrodynamics, Nature Phys. **19**, 394 (2023).

[13] J. Niu, L. Zhang, Y. Liu, J. Qiu, W. Huang, J. Huang, H. Jia, J. Liu, Z. Tao, W. Wei, Y. Zhou, W. Zou, Y. Chen, X. Deng, X. Deng, C. Hu, L. Hu, J. Li, D. Tan, Y. Xu, F. Yan, T. Yan, S. Liu, Y. Zhong, A. N. Cleland, and D. Yu, Low-loss interconnects for modular superconducting quantum processors, Nature Electron. **6**, 235 (2023).

[14] Y. P. Zhong, H.-S. Chang, K. J. Satzinger, M.-H. Chou, A. Bienfait, C. R. Conner, Ã. Dumur, J. Grebel, G. A. Peairs, R. G. Povey, D. I. Schuster, and A. N. Cleland, Violating Bell's in-

equality with remotely connected superconducting qubits, Nat. Phys. **15**, 741 (2019).

[15] S. Storz, J. Schär, A. Kulikov, P. Magnard, P. Kurpiers, J. Lütolf, T. Walter, A. Copetudo, K. Reuer, A. Akin, J.-C. Besse, M. Gabureac, G. J. Norris, A. Rosario, F. Martin, J. Martinez, W. Amaya, M. W. Mitchell, C. Abellan, J.-D. Bancal, N. Sangouard, B. Royer, A. Blais, and A. Wallraff, Loophole-free bell inequality violation with superconducting circuits, Nature (London) **617**, 265 (2023).

[16] Z. K. Minev, T. G. McConkey, M. Takita, A. D. Corcoles, and J. M. Gambetta, Circuit quantum electrodynamics (cQED) with modular quasi-lumped models, arXiv:2103.10344 [cond-mat, physics:quant-ph].

[17] J. J. G. Ripoll, *Quantum Information and Quantum Optics with Superconducting Circuits* (Cambridge University Press, Cambridge, 2021).

[18] G. Johansson, L. Tornberg, V. S. Shumeiko, and G. Wendin, Readout methods and devices for josephson-junction-based solid-state qubits, J. Phys.: Condens. Matter **18**, S901 (2006).

[19] B. Peropadre, J. Lindkvist, I.-C. Hoi, C. M. Wilson, J. J. Garcia-Ripoll, P. Delsing, and G. Johansson, Scattering of coherent states on a single artificial atom, New J. Phys. **15**, 035009 (2013).

[20] M. Bamba and T. Ogawa, Recipe for the Hamiltonian of system-environment coupling applicable to the ultrastrong-light-matter-interaction regime, Phys. Rev. A **89**, 023817 (2014).

[21] M. Malekakhlagh and H. E. Türeci, Origin and implications of an A^2-like contribution in the quantization of circuit-QED systems, Phys. Rev. A **93**, 012120 (2016).

[22] J. Bourassa, J. M. Gambetta, A. A. Abdumalikov, O. Astafiev, Y. Nakamura, and A. Blais, Ultrastrong coupling regime of cavity QED with phase-biased flux qubits, Phys. Rev. A **80**, 032109 (2009).

[23] S. E. Nigg, H. Paik, B. Vlastakis, G. Kirchmair, S. Shankar, L. Frunzio, M. H. Devoret, R. J. Schoelkopf, and S. M. Girvin, Black-Box superconducting circuit quantization, Phys. Rev. Lett. **108**, 240502 (2012).

[24] F. Solgun and D. P. DiVincenzo, Multiport impedance quantization, Ann. Phys. (NY) **361**, 605 (2015).

[25] C. W. Gardiner and P. Zoller, *Quantum Noise* (Springer, Berlin, 2004).

[26] B. Abdo, A. Kamal, and M. Devoret, Nondegenerate three-wave mixing with the Josephson ring modulator, Phys. Rev. B **87**, 014508 (2013).

[27] J. I. Cirac, P. Zoller, H. J. Kimble, and H. Mabuchi, Quantum state transfer and entanglement distribution among distant nodes in a quantum network, Phys. Rev. Lett. **78**, 3221 (1997).

[28] C. W. Gardiner and M. J. Collett, Input and output in damped quantum systems: Quantum stochastic differential equations and the master equation, Phys. Rev. A **31**, 3761 (1985).

[29] C. Forestiere and G. Miano, Phys. Scr. **99**, 045123 (2024).

[30] B. Yurke and J. S. Denker, Quantum network theory, Phys. Rev. A **29**, 1419 (1984).

[31] C. M. Bender and D. H. Sharp, Solution of operator field equations by the method of finite elements, Phys. Rev. Lett. **50**, 1535 (1983).

[32] M. Razavy, *Heisenberg's Quantum Mechanics* (World Scientific, Singapore, 2011).